RSC Publishing Faraday Discussions

Evaluating the impacts of amino acids in the second and outer coordination spheres of Rh bis(diphosphine) complexes for CO2 hydrogenation

Journal:	*Faraday Discussions*
Manuscript ID	FD-ART-11-2018-000164
Article Type:	Paper
Date Submitted by the Author:	04-Nov-2018

Complete List of Authors:	Walsh, Aaron; Pacific Northwest National Lab Laureanti, Joseph; Pacific Northwest National Lab Katipamula, Sriram; Pacific Northwest National Lab Chambers, Geoffrey; Pacific Northwest National Laboratory, Chemical and Materials Sciences Priyadarshani, Nilusha; Pacific Northwest National Lab Lense, Sheri; Pacific Northwest National Lab Bays, Tim; Pacific Northwest National Laboratory, Linehan, John; Pacific Northwest National Laboratory, Catalysis Science Group, Fundamental & Computational Sciences Shaw, Wendy; Pacific Northwest National Lab,

Evaluating the impacts of amino acids in the second and outer coordination spheres of Rh-bis(diphosphine) complexes for CO_2 hydrogenation

Aaron P. Walsh[a†], Joseph A. Laureanti[a†], Sriram Katipamula[b], Geoffrey M. Chambers, Nilusha Priyadarshani[c], Sheri Lense[d], J. Timothy Bays, John C. Linehan, Wendy J. Shaw*

[†]Authors contributed equally to this work.

[a]Physical and Computational Sciences Directorate, Pacific Northwest National Laboratory, Richland, WA 99352, USA.

[a]Current address: Ferro Corporation, Penn Yan, NY 14527

[b]Current address: Rutgers University, Piscataway, NJ 08854

[c]Current address: Curium, Maryland Heights, MO

[d]Current address: University of Wisconsin-Oshkosh, Oshkosh, WI

Abstract

To explore the influence of a biologically inspired second and outer coordination sphere on Rh-bis(diphosphine) CO_2 hydrogenation catalysts, a series of five complexes were prepared by varying substituents on the pendant amine in the $P(Et)_2CH_2N^RCH_2P(Et)_2$ ligands ($P^{Et}N^RP^{Et}$), where R consists of methyl ester modified amino acids, including three neutral (glycine methyl ester (GlyOMe), leucine methyl ester (LeuOMe), phenylalanine methyl ester (PheOMe)), one acidic (aspartic acid dimethyl ester (AspOMe)) and one basic (histidine methyl ester (MeHisOMe)) amino acid esters. The turn over frequencies (TOFs) for CO_2 hydrogenation for each of these complexes was compared to the non-amino acid containing $[Rh(depp)_2]^+$ (depp) and $[Rh(P^{Et}N^{Me}P^{Et})_2]^+$ (NMe) complexes. Each complex is catalytically active for CO_2 hydrogenation to formate under mild conditions in THF. Catalytic activity spanned a factor of four, with the most active species being the NMe catalyst, while the slowest were the GlyOMe and the AspOMe

complexes. When compared to a similar set of catalysts with phenyl-substituted phosphorous groups, a clear contribution of the outer coordination sphere is seen for this family of CO_2 hydrogenation catalysts.

Introduction

Enzymes are able to convert small molecules selectively, efficiently, and with minimal energy input.[1-4] These complex biological catalysts often feature metallic centers within highly tuned coordination environments with intricate second and higher order coordination sphere architecture that facilitate this incredible performance. Research focused on molecular catalysts has strived to achieve the efficacy of enzymes, primarily by modifying the first coordination sphere, the ligands bound to the metal. The second coordination sphere, which is comprised of functional groups which can interact with the metal but aren't bound to the metal, have been instrumental in many of the more recent advancements.[5-7] In spite of these advancements, however, the majority of synthetic catalysts still fall short of enzymatic performance.[8-11] The introduction of outer coordination sphere functionality to small molecule catalysts has proven advantageous in some cases, demonstrating that the bioinspired approach to molecular catalyst design is a viable path to achieve similar catalytic performance.[12-15]

Our previous work with hydrogen oxidation catalysts demonstrated the positive impact of including an outer coordination sphere.[11,16] Using attributes beyond the first and second coordination sphere, we were able to achieve faster TOFs,[17,18] lower overpotentials,[19,20] and electrochemically reversible catalysis while maintaining fast TOFs.[16,21,22] Cooperativity between the first, second, and outer coordination spheres are vital, and the performance is highly sensitive to modest changes due to possible disruption between intersphere cooperativity.[16,17,23]

In this work, we directly incorporate amino acid analogs into the outer coordination sphere of molecular catalysts for CO_2 hydrogenation. The conversion of CO_2 has potential importance in energy storage and higher value products, as well as controlling adverse climate effects. The use of second coordination sphere elements in CO_2 reduction has been addressed by us and others. As examples, Fujita and coworkers introduced water soluble ligands allowing the transformation of CO_2 to formate in aqueous solution by iridium complexes, with a protonatable group facilitating CO_2 addition and reduction.[24,25] Kubiak investigated pendant amines in the second coordination spheres using a P_2N_2 framework with rhodium and found the steric bulk of the pendant amine substituent hindered catalysis.[26] Nilay and co-workers introduced PNP-pincer ligands to iridium and showed that ^{13}C-labeled carbon dioxide will directly bind to the iridium metal center with the assistance of a hydrogen bond donor in the second coordination sphere.[27]

Little effort has been focused on the outer coordination sphere of CO_2 hydrogenation catalysts. We provided one such study, investigating a series of $[Rh(P^{Ph}N^{R}P^{Ph})_2]^+$ complexes as a function of the pendant amine substituent.[28] These complexes were extremely sensitive to both a pendant amine in the second coordination sphere, and changes in the outer coordination sphere by altering the R group, with TOFs spanning two orders of magnitude. However the amino acid ester and dipeptide complexes were very slow (~10 hr^{-1}), adding experimental difficulty in collecting the data. Given the thermodynamics of this system, our expectation was that alkyl-substituted phosphorous groups would result in faster catalysts,[29,30] allowing us to more readily implement and evaluate the impact of the outer coordination sphere on various points in the proposed catalytic cycle (Figure 1). Consequently, in this work, we evaluated the analogous $[Rh(P^{Et}N^{R}P^{Et})_2]^+$ complexes to allow implementation of a more complex outer coordination sphere. We investigated

the role of the pendant amine with just a methyl group, as well as a series of amino acid esters substituents on the pendant amine.

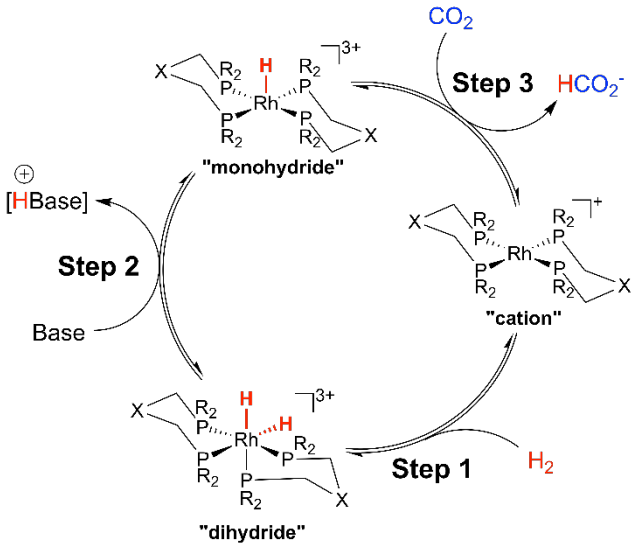

Figure 1. Proposed mechanism for catalytic hydrogenation of carbon dioxide by the $[Rh(PN^{R}P)_2][BF_4]$ catalysts in organic solvents.

Results

Synthesis of N,N-Bis(diethyphosphino)Amino Acid Methyl Ester ($PN^{R}P$) Ligands and Metal Complexes. To determine the impact of amino acid residues in the outer-coordination sphere on catalytic performance, five new $[Rh(PN^{R}P)_2][BF_4]$ complexes were prepared with different substituents off the N group (Figure 2), where N^{R} is N-$CH(CH_2COOCH_3)COOCH_3$ (aspartic acid dimethyl ester, AspOMe), N-CH_2COOCH_3 (glycine methyl ester, GlyOMe), N-$CH(CH_2CH(CH_3)_2)COOCH_3$ (leucine methyl ester, LeuOMe), N-$CH(CH_2C_6H_5)COOCH_3$ (phenylalanine methyl ester, PheOMe), and N-$CH(CH_2C_4H_6N_2)COOCH_3$ (histidine methyl ester, MeHisOMe). The simpler $Rh(PN^{Me}P)_2$ and $Rh(depp)_2$[31] (depp=diethyl phosphino propane)[32] complexes, were also investigated to probe the mechanism for CO_2 hydrogenation. Neutralized

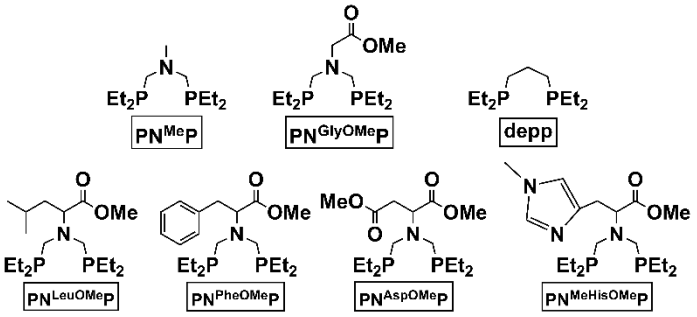

Figure 2. PNP ligands and their abbreviations.

methyl ester protected amino acids were condensed with (hydroxylmethyl)diethylphosphine in anhydrous ethanol to produce PN^RP ligands (Scheme 1)[33] generally in good yield (>70%). The addition of $[Rh(COD)_2][BF_4]$ in tetrahydrofuran (THF) to two equivalents of ligand resulted in powders of metal complex generally in good yield (>60%) after precipitation from a concentrated solution. Ligands and complexes were characterized by ^{31}P and ^{1}H nuclear magnetic resonance (NMR) spectroscopy, and elemental analysis; metal complexes were also characterized by electrochemistry as well as single crystal x-ray diffraction. The resulting metal complexes display a characteristic doublet in the $^{31}P\{^{1}H\}$ NMR spectra between 3.5 and 6.0 ppm, corresponding to the Rh-P coupling ($^{1}J_{Rh\text{-}P}$ = 125.5±0.5 Hz, Table 1 and Figure 3, bottom and Figure S1) and show dihydrides with the addition of H_2 (Figure 3 and S2), as expected.

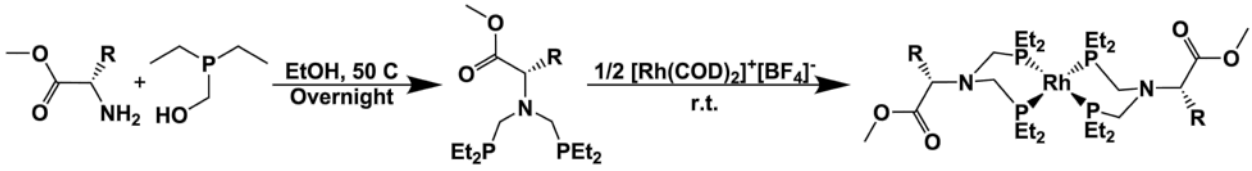

Scheme 1. Overall synthesis of amino acid ester incorporated PNP ligands and metal complexes.

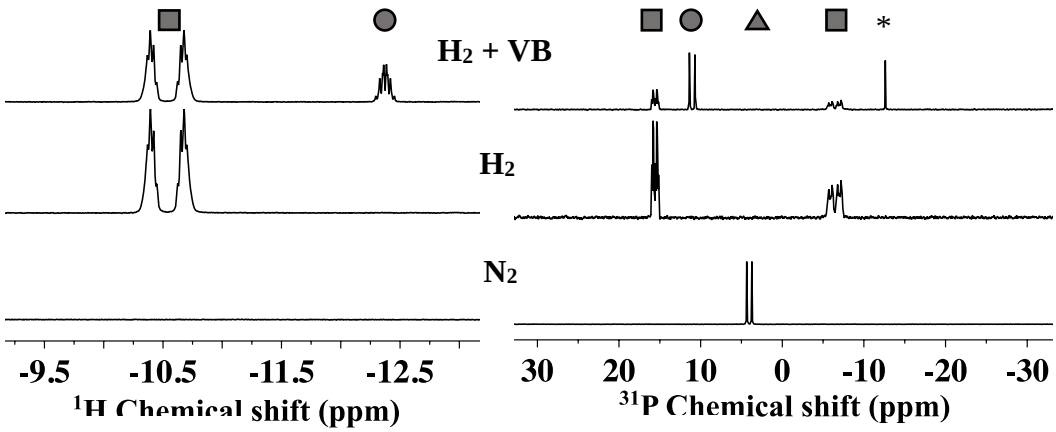

Figure 3. Representative chemical shifts, ^{1}H (left) and $^{31}P\{^{1}H\}$ (right), for $[Rh(PN^{R}P)_2]^+$ complexes under 1 atm N_2 (bottom) or $[Rh(PN^{R}P)_2]^+$ complexes under 1 atm H_2 in the absence ($[(H)_2Rh(PN^{R}P)_2]^+$; middle) and presence ($[(H)Rh(PN^{R}P)_2]$; top) of 1.1 equivalents of Verkade's base (VB). Resonances are denoted as follows: squares=dihydride, circles=monohydride, and triangles=cationic species. * denotes protonated Verkade's base.

Table 1. ^{1}H and $^{31}P\{^{1}H\}$ NMR chemical shifts and *J*-couplings, and reduction potentials for $[Rh(PN^{R}P)_2]^+$ under nitrogen and under H_2 in the presence ($[(H)Rh(PN^{R}P)_2]$) and absence ($[(H)_2Rh(PN^{R}P)_2]^+$) of Verkade's base. n/a and n/d denote not applicable and not determined, respectively.

Complex	$^{31}P\{^{1}H\}$ NMR (ppm)	$^{1}J_{RhP}$ (Hz)	^{1}H NMR hydride (ppm)	$^{1}J_{RhH}$ (Hz)	$E_{p,a}$ (V vs Fc)
$[Rh(PN^{Phe}P)_2]^+$	4.65	125.7	n/a	n/a	0.23
$[Rh(PN^{Me}P)_2]^+$	5.46	125.2	n/a	n/a	0.11
$[Rh(PN^{MeHis}P)_2]^+$	4.04	125.6	n/a	n/a	0.46
$[Rh(PN^{Leu}P)_2]^+$	4.21	125.2	n/a	n/a	0.3
$[Rh(depp)_2]^+$	5.99	126.6	n/a	n/a	0.14
$[Rh(PN^{Asp}P)_2]^+$	4.46	125.5	n/a	n/a	0.35
$[Rh(PN^{Gly}P)_2]^+$	3.87	125.4	n/a	n/a	0.07
$[(H)_2Rh(PN^{Phe}P)_2]^+$	17.31, -4.39	*a*, *a*	-10.52	145	0.71
$[(H)_2Rh(PN^{Me}P)_2]^+$	18.89, -3.99	*a*, *a*	-10.5	145	0.55
$[(H)_2Rh(PN^{MeHis}P)_2]^+$	16.49, -5.51	93.7, *a*	-10.54	145	0.69
$[(H)_2Rh(PN^{Leu}P)_2]^+$	16.97, -4.51	94.1, *a*	-10.49	145	0.81
$[(H)_2Rh(depp)_2]^+$	14.92, -6.52	93.4, 82.0	-10.75	145	0.87
$[(H)_2Rh(PN^{Asp}P)_2]^+$	17.05, -4.58	*a*, *a*	-10.53	145	0.79
$[(H)_2Rh(PN^{Gly}P)_2]^+$	17.93, -4.08	93.9, 82.6	-10.46	145	0.63
$[(H)Rh(PN^{Phe}P)_2]$	12.23	139.4	-12.34	140	nd
$[(H)Rh(PN^{Me}P)_2]$	12.38	139.4	-12.3	140	nd
$[(H)Rh(PN^{MeHis}P)_2]$	11.95	139.2	-12.37	145	nd
$[(H)Rh(PN^{Leu}P)_2]$	11.89	139.2	-12.39	145	nd

[(H)Rh(depp)$_2$]	10.96	139.4	-12.67	145	nd
[(H)Rh(PN^{Asp}P)$_2$]	12.1	139.4	-12.39	145	nd
[(H)Rh(PN^{Gly}P)$_2$]	12.18	139.2	-12.32	140	nd

[a]Poorly resolved.

Catalytic Hydrogenation of Carbon Dioxide. All of the complexes evaluated were active for catalytic hydrogenation of CO_2 to formate at room temperature and 34 atm of 1:1 CO_2:H_2 in the presence of Verkade's base (2,8,9-triisopropyl-2,5,8,9-tetraaza-1-phosphabicyclo[3.3.3]undecane) in THF-d_8. Catalytic performance was evaluated using the TOF for each complex (Table 2, Figure 4). Observed TOFs for the [Rh(PN^{R}P)$_2$]$^+$ catalysts decrease in the following order: NMe > LeuOMe > MeHisOMe > PheOMe > GlyOMe > AspOMe. Product formation was monitored using operando ^{1}H NMR spectroscopy and quantified using the residual HDO resonance from a capillary insert of D_2O as standard, containing $CoCl_2$ as a relaxation agent to shift the resonance to provide spectral resolution. Catalytic runs exhausted the Verkade's base confirmed by the loss of the original ^{31}P{^{1}H} resonance at 120 ppm, and replacement by the protonated Verkade's base resonance at ~-12 ppm in the ^{31}P{^{1}H} NMR spectrum.

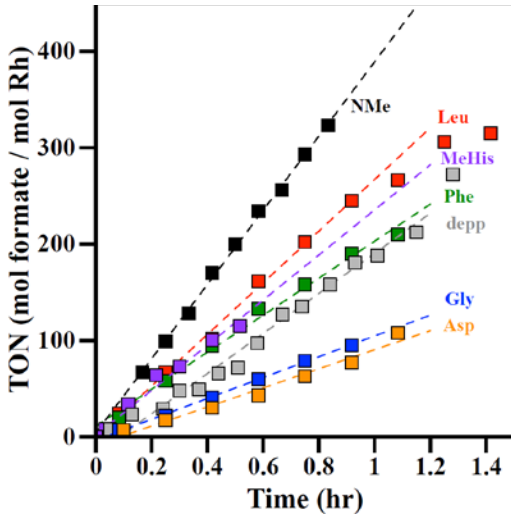

Figure 4. Representative plots of the production of formate as a function of time, determined for the complexes in this study from operando ^{1}H NMR spectroscopy. Black=NMe, red=LeuOMe, green=PheOMe, purple=MeHisOMe, grey=depp, blue=GlyOMe, and orange=AspOMe. Reaction conditions: [Rh(PN^{R}P)$_2$]$^+$ (1.0 mM), 1:1 CO_2:H_2, 34 atm, THF-d_8, Verkade's base (515±40 mM).

Table 2. TOF of formate production using $[Rh(PN^RP)_2]^+$ catalysts. Catalyst loading was 1.0 mM under 34 atm 1:1 CO_2:H_2.

$[Rh(P^{Et}N^RP^{Et})_2]^+$ Catalyst, R =	**TOF (hr^{-1})**	**Equivalents Verkade's base for Ethyl-substituted**	**TOF for $[Rh(P^{Ph}N^RP^{Ph})_2]^{+a}$**
NMe	420 (60)	550 (80)	920 (20)[a]
MeHisOMe	250 (20)	500	NA
LeuOMe	245 (60)	450 (105)	NA
PheOMe	200 (30)	500 (25)	NA
depp/dppp (no N)	170 (20)	500	150 (50)[a]
GlyOMe	100 (20)	520 (10)	11 (4)[a]
AspOMe	100 (25)	410 (150)	NA
Gly	NA	NA	120 (10)[a]
GlyAlaOMe	NA	NA	12 (7)[a]

[a]Reported in reference [28]

Thermodynamic Studies. Thermodynamic parameters were determined by evaluating the addition of H_2 to form the dihydride and then the addition of base to form the monohydride under lower pressures and concentrations. In all cases for the ethyl-substituted complexes in this study, exposure to 1 atm of H_2 results in 100% conversion to the dihydride species, with a representative spectrum shown in Figure 3 and others shown in Figures S1 and S2, and a crystal structure for the NMe complex shown in Figure 5 with selected distances shown in Table S1. Upon the addition of Verkade's base, the dihydride is deprotonated to monohydride, with 3 – 5 equivalents resulting in complete deprotonation (Figure 3, S1 and S2). The data with one equivalent of added Verkade's

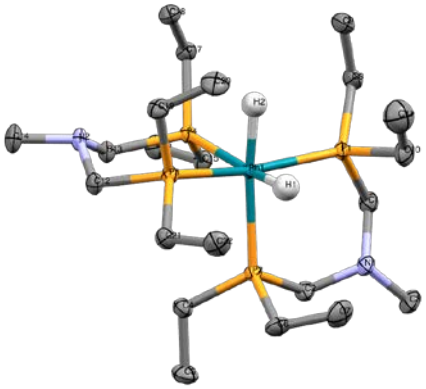

Figure 5. Crystal structure of the $[(H)_2Rh(P^{Et}N^{Me}P^{Et})_2]^+$ complex shown with ellipsoids at 50% probability. Anions, solvent molecules and hydrogens are not shown for clarity.

were used to estimate pK_a values that show an average of 33.3±0.5, and average hydricities of 26.8±0.6 kcal/mol, respectively, assuming a K_{eq}>100 for the H_2 addition step (Table 3).

Table 3. Thermodynamic parameters for $[Rh(P^RN^{R'}P^R)_2]^+$ complexes.

Catalyst	pK_a	ΔG_{H-}
$[Rh(P^{Et}N^{AspOMe}P^{Et})_2]^+$	33.4	25.9
$[Rh(P^{Et}N^{LeuOMe}P^{Et})_2]^+$	33.8	26.1
$[Rh(P^{Et}N^{Me}P^{Et})_2]^+$	32.8	26.7
$[Rh(P^{Et}N^{GlyOMe}P^{Et})_2]^+$	33.3	26.9
$[Rh(P^{Et}N^{PheOMe}P^{Et})_2]^+$	33.7	27.0
$[Rh(P^{Et}N^{MeHisOMe}P^{Et})_2]^+$	33.5	27.3
$[Rh(P^{Et}N^{depp}P^{Et})_2]^+$	32.7	27.4
$[Rh(P^{Ph}N^{GlyOMe}P^{Ph})_2]^+$ [a]	31.7 [a]	27.7[a]

[a]Reported in reference [28]

Electrochemical analysis of [Rh(PN^{R}P)$_2$][BF$_4$] Complexes. Cyclic voltammetry experiments were employed to directly interrogate the electronic properties of the $[Rh(PN^RP)_2]^+$ and $[(H)_2Rh(PN^RP)_2]^+$ species under 1.0 atmosphere of nitrogen or hydrogen, respectively, in a solution of [TBA][BF4] (0.1 M) in THF. Voltammograms were first recorded under a nitrogen atmosphere with the $[Rh(PN^RP)_2]^+$ at ~1.0 mM, Figure 6. Hydrogen was then sparged through the solution, resulting in the rapid formation of the dihydride, confirmed by the bleaching of the solution from yellow to colorless. Under an atmosphere of nitrogen, one irreversible oxidation is observed that is attributed to the Rh^{III}/Rh^I couple (i.e. oxidation of the 16-electron Rh^I cation to a 14-electron Rh^{III} species).[34] Similar electrochemical behavior is observed under an atmosphere of hydrogen, with the exception of shifts of the anodic peak potential (E_{pa}) of, on average, 0.5±0.025 V in the anodic direction. The oxidation events under hydrogen are attributed to the oxidation of the Rh^{III}-dihydride species to a Rh^I cationic species and are irreversible in all cases.

Plots of the E_{pa} for the irreversible oxidation of the Rh^{I+} species vs. the respective chemical shifts in the $^{31}P\{^1H\}$ NMR produces a linear trend, suggesting that the electron density reported by the

^{31}P NMR reflects the electron density at the metal. Specifically, as electron density is increasingly removed from the rhodium metal and redirected to the phosphorus atoms, a concomitant shift to more positive potentials for the E_{pa} is observed as well as an upfield shift of the resonance in the $^{31}P\{^{1}H\}$ NMR (Figure S3). However, there is no correlation between the observed catalytic CO_2 hydrogenation TOFs and either the E_{pa} or the $^{31}P\{^{1}H\}$ chemical shift of the $[Rh(PN^{R}P)_2]^+$, Figure S4.

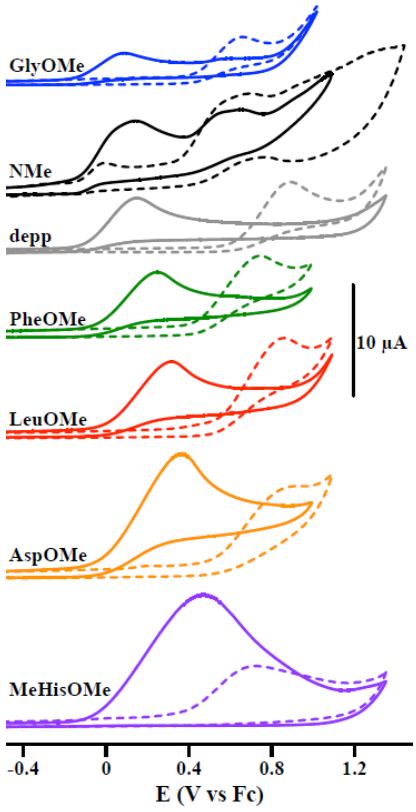

Figure 6. Cyclic voltammetry of the $[Rh(P^{Et}N^{R}P^{Et})_2]^+$ complexes under N_2 (solid) and H_2 (dashed), recorded in THF at 0.2 V s^{-1}.

Discussion

General methods for modulating catalytic activity of homogenous catalysts rely on substitution of the atoms directly coordinating a metal, and varying the electron donating and withdrawing effects of the substituents of these primary coordinating atoms. An alternative strategy is to manipulate the second and outer coordination sphere interactions of the metal, which has been shown to increase the catalytic activity by several orders of magnitude for proton reduction and hydrogen oxidation catalysts, as well as to improve the catalytic efficiency.[7,14-16,25-27,35-41] The influence of the second coordination sphere has been addressed for catalysts for CO_2 reduction,[7,25-27,36,40,41] but less of an influence of the outer coordination sphere. In this work, we investigate the role of a bioinspired second and outer coordination sphere for CO_2 hydrogenation catalysts, where the role of a secondary coordination sphere pendant amine is investigated, and the outer coordination sphere is modulated by substitution of various amino acid ester analogues at the pendant amine.

The TOFs for CO_2 hydrogenation using the seven complexes in this study span a range of four-fold. The pendant amine has a modest impact in these complexes, with an almost two-fold increase in TOF for the NMe complex compared to the depp complex. For complexes containing a pendant amine, the NMe derivative is the fastest (400 hr^{-1}), while the GlyOMe and AspOMe complexes are the slowest (100 hr^{-1}). While the NMe complex is the least bulky and is also the fastest, the order of TOFs is not clearly associated with steric bulk, since the GlyOMe complex, which has the smallest side chain, is also the slowest. Further, our combined electrochemical and ^{31}P NMR studies suggest that there is not a pure correlation between the TOF and the electron density at the metal (Figure S4). In most of the analyses of TOF vs. another observable, there is often a qualitative correlation with the exception of a couple of points. Unfortunately, the data

points that don't correlate are different for each observable. For instance, NMe and AspOMe complexes stand out from the trend for electron density at the metal, while the chemical shift of the ^{31}P resonance is clearly out of line for the depp complex. Overall, the modest change as a function of outer coordination sphere functional group suggests a minimal impact of the outer coordination sphere when considering this data in isolation.

Influence of the phosphorous substituent. To more fully assess the impact of the outer coordination sphere on this series of complexes, we consider a similar family of complexes that was studied, with phenyl substituents on the phosphorous atom rather than ethyl groups.[28] In that series of complexes, the differences in TOF as a function of side chain were stark; some of TOFs are reproduced in Table 2. For instance, the addition of the pendant amine resulted in an order of magnitude increase in TOF, while addition of an amino acid slowed the TOF by an order of magnitude, and complexes with the addition of amino acid esters or dipeptides slowed the TOF by two orders of magnitude with respect to the NMe complex. There are two issues of interest to compare. The first is why there was such a significant impact on the TOFs of the phenyl-substituted complexes and not on the ethyl-substituted complexes. The second is a comparison of phenyl-substituted and ethyl-substituted complexes with similar functional groups.

The source of the impact on Phenyl-substituted complexes. The phenyl-substituted complexes are expected to have slower TOFs based on the high hydricity of the bis-diphosphine substituted Rh complexes as a result of the aromatic substituents.[29,30] The range of TOFs for the ethyl-substituted complexes (100-400 hr^{-1}) was generally faster than that of the phenyl-substituted complexes (12-920 hr^{-1}), with the exception of the phenyl-substituted NMe complex which is at least a factor of two faster than all other complexes (Table 2).[28]

The lower hydricity and higher pK_a of the Rh-dihydride in the ethyl-substituted complexes (Table 3) may result in a difference in the rate limiting step. This possibility was investigated by looking at each step under stoichiometric conditions. In all cases for the ethyl-substituted complexes in this study, exposure to 1 atm of H_2 results in 100% conversion to the dihydride species (Figure S1 and S2), while addition of base gave a distribution of dihydride and monohydride. In contrast, the phenyl-substituted complexes added H_2 very poorly. ΔG_{H2} values ranged from 0.41 to 1.44 kcal/mol for phenyl-substituted complexes containing a pendant amine, representing < 10% conversion upon exposure to 1 atm of H_2.[28] However, upon addition of 3-5 eq of Verkade's base, complete conversion to the monohydride was observed. Based on this data, we determined that the pK_a values for the ethyl-substituted complexes are slightly higher than that observed for the phenyl-substituted complexes (Table 3), while the hydricities are lower. Both of these observations suggest that it should be harder to deprotonate the dihydride of the ethyl-substituted complexes. Note that no monohydride was observed in the absence of added base in either complex, consistent with our expectation that the pK_a of the pendant amine is too acidic to deprotonate the dihydride species on its own.

The phenyl-substituted complexes were proposed to proceed through the catalytic cycle shown in Figure 1 with the rate limiting step being the CO_2 to HCO_2^- conversion. Based on the thermodynamic parameters determined for the observations of the ethyl-substituted complexes (Table 3), it is possible that the rate limiting step switches from the CO_2 conversion to formate in the phenyl-substituted complexes (Step 3 in Figure 1) to deprotonation of the dihydride in the ethyl-substituted complexes (Step 2 in Figure 1). The collective data from the studies of the phenyl-substituted complexes and the ethyl-substituted complexes imply that the role of the pendant amine

and the outer coordination sphere in the phenyl-substituted complexes was facilitating the addition of CO_2/conversion to formate (Step 3), rather than influencing deprotonation.

Comparison of phenyl-substituted and ethyl-substituted analogs. Comparison of analogous ethyl- and phenyl substituted complexes supports a role of the outer coordination sphere. In the two sets of complexes, we have three analogous complexes, with the only difference being the substituent on the phosphorous atoms. These are the depp/dppp complexes, the NMe complexes, and the GlyOMe complexes. While we do expect an effect from the primary coordination sphere, if the only effect were the primary coordination sphere,[29,30] we would expect a similar influence regardless of the second and outer coordination spheres; however, we see differing effects due to the second and outer coordination spheres (Figure 6), pointing to a clear role. Specifically, in the NMe set of complexes, the TOF of the phenyl-substituted complex is two-times faster than the ethyl-substituted, while for the GlyOMe complexes, the phenyl-substituted complex is ten-times slower than the ethyl-substituted complex. For the depp/dppp complexes, the TOFs are the same, within error. We would anticipate that the phenyl-substituted would always be slower if the primary coordination sphere was the dominant factor;[29,30] instead we observe that they are sometimes slower and sometimes faster, by significantly different amounts, and only with the presence of the pendant amine. These observations suggest that the phosphorous substituents are not responsible for the observed effect, and consequently implicate the outer coordination sphere in contributing to the catalytic TOF. Computational and experimental studies are ongoing to understand the individual or multiple contributions of the outer coordination sphere.

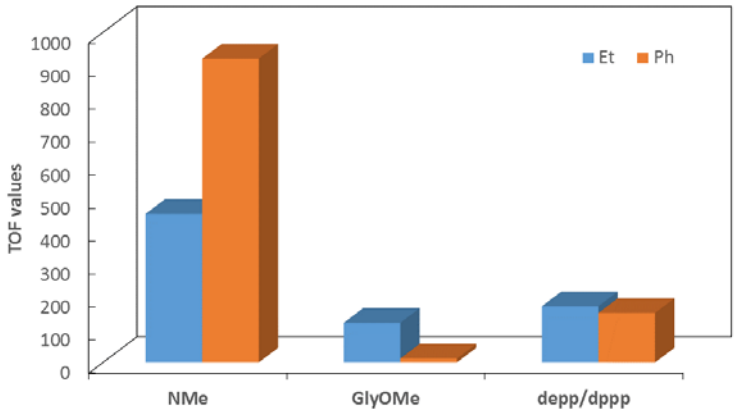

Figure 7. Observed TOF values of analogous ethyl-substituted (this work) and phenyl-substituted complexes. The different relative rates for complexes substituted differently on the bridge atom (C or N) suggest effects beyond the primary coordination sphere.

Conclusion

This series of Rh complexes for CO_2 hydrogenation shows a clear impact of the outer coordination sphere, particularly when compared to the analogous phenyl-substituted complexes. The TOFs of the ethyl-substituted complexes, the complexes that are the focus of this study, span a modest range of a factor of four as a function of amino acid modification. However, when compared to their complementary phenyl-substituted complexes, the TOFs are either 10x slower, 2x faster, or exactly the same, behavior that would not be observed if the primary coordination sphere was the only contribution to the mechanism. The mechanism or mechanisms that are driving this behavior are still under investigation, but this data points to this system being a rich system for investigation of the effects of the outer coordination sphere.

Methods

General Procedures.

All experiments were conducted under a nitrogen atmosphere inside a Vacuum Atmospheres glovebox or on a Schlenk line unless otherwise noted. All chemicals purchased were of the highest purity commercially available and used as received unless otherwise noted. A NaK alloy was used to dry THF-d_8, which was then distilled under vacuum. Acetonitrile, diethyl ether, dichloromethane, ethanol, and tetrahydrofuran were purified by passage through activated alumina columns in an Innovative Technology, Inc. PS-MD-6 solvent purification system. UHP (ultra high purity) CO_2, H_2, and gas mixtures were purchased from Oxarc. Polyetheretherketone (PEEK) cells were employed for use with high pressure catalysis using *operando* NMR spectroscopy, designed and constructed at the Pacific Northwest National Laboratory.[42] All NMR spectroscopy data was collected on a Varian NMRS or Inova operating at 500 MHz ^{1}H frequency. Chemical shift values for $^{31}P\{^1H\}$ NMR spectra were referenced to an external 85% H_3PO_4 standard at 0 ppm. Elemental analysis was performed at by the CENTC Elemental Analysis Facility at the University of Rochester. For the crystal structure characterization, a suitable crystal was selected, mounted on a MiTeGen MicroMounts pin using Paratone-N oil, and cooled to the data collection temperature (140(2)) K. Data was collected on a Bruker-AXS II CCD diffractometer with 0.71073 Å Mo Kα radiation. Cell parameters were retrieved using Bruker APEX II software,[43] raw data were integrated using SAINTPlus,[44] and absorption correction was applied using SADABS.[45] The structure was solved using direct methods and refined by a least-squares method on F^2 using SHELXS-97 and SHELXL-97,[46] respectively, as well as SHELXL-2018/3 to improve the structure refinement,[47] using the OLEX2 software package as a front end.[48]

Synthetic Procedures.

General procedure for the neutralization for amino acid methyl esters. Neutralization was conducted in a manner similar to previously described methods.[33] Methyl ester-protected amino

acids were purchased as the hydrochloride salt, 1.0 equiv, 5.28 mmol was added to a Morton flask, and dissolved in 20 mL of dichloromethane. Sodium carbonate was added as a solution in water (10.0 equiv, 52.8 mmol), and the resulting mixture was stirred vigorously for 20 minutes. The organic layer was separated and, combined with anhydrous $MgSO_4$ (5.0 g, 40 mmol), and stirred an additional five minutes to remove any residual water. $MgSO_4$ was then collected over a frit, and the solvent was removed from the organic layer via reduced pressure. Final products were isolated as a clear, high-boiling oils, and used without further characterization.

General procedure for the synthesis of PN^RP ligand. The syntheses of all PN^RP ligands used in this study were performed in a manner similar to previously described methods[3]. Briefly, diethylphosphinomethanol (0.24 g, 2 mmol) was prepared using a modified preparation from that previously reported,[32] specifically, diethylphosphine (5.0 g, 55.5 mmol) and paraformaldehyde (1.665 g, 55.4 mmol) were dissolved in 0.05 L of absolute ethanol and the ensuing reaction mixture was stirred overnight at 60°C under a nitrogen atmosphere. Removal of the solvent under reduced pressure afforded a colorless oil. The resulting alcohol and the neutralized amino acid ester (1 mmol) were dissolved in 25 mL of absolute ethanol in a 50 mL Schlenk flask equipped with a stir bar. Reactions were heated to 50-60 °C for 16 hours under nitrogen, after which the flask was cooled and the solvent was removed under reduced pressure to obtain a colorless oil. Ligands were obtained in >70% yield.

$PN^{LeuOMe}P$. The leucine methyl ester (LeuOMe) ligand: ^{1}H NMR (500 MHz, THF-d_8): δ 4.12 (m, 1H), 3.61 (s, 3H), 3.08 (dd, 2H), 2.63 (dd, 2H), 1.49 (m, 4H), 1.35 (m, 8H), 1.05 (m, 12H), 0.93 (m, 6H). ^{31}P{^{1}H} NMR (202MHz, THF-d_8): δ -30.49 Anal. Calcd (found) for $C_{17}H_{37}NO_2P_2$: C, 58.43 (58.6); H, 10.67 (10.92); N, 4.01 (3.72).

$PN^{AspOM}P$ –The aspartic acid methyl ester (AspOMe) ligand: ^{1}H NMR (500 MHz, THF-d_8): δ 3.63 (s, 3H), 3.58 (s, 3H), 2.97 (d, 2H), 2.79 (dd, 1H), 2.58 (ddd, 4H), 1.34 (m, 8H), 1.04 (m,

12H). $^{31}P\{^{1}H\}$ NMR (202MHz, THF-d_8): δ -30.7. Anal. Calcd (found) for $C_{16}H_{33}NO_4P_2$: C, 52.59 (52.92); H, 9.1 (9.03); N, 3.83 (3.78).

$PN^{GlyOMe}P$. The glycine methyl ester (GlyOMe) ligand: ^{1}H NMR (500 MHz, THF-d_8): δ 3.62 (s, 3H), 3.35 (s, 2H), 2.92 (s, 4H), 1.37 (q, 8H, J_H = 7.81 Hz), 1.05 (t, 12H, J_H = 7.62 Hz. $^{31}P\{^{1}H\}$ NMR (202MHz, THF-d_8): δ -30.9 ppm (s). Anal. Calcd (found) for $C_{13}H_{29}NO_2P_2$: C, 53.23 (53.63); H, 9.96 (10.4); N, 4.77 (4.73).

$PN^{PheOMe}P \bullet ½\ H_2O$. The phenylalanine methyl ester (PheOMe) ligand: ^{1}H NMR (500 MHz, THF-d_8): δ 7.22 (m,5H), 3.78 (m, 1H), 3.63 (s, 3H), 3.16 (q, 4H), 3.01 (dd, 2H), 1.83 (m, 8H), 1.17 (m, 12H). $^{31}P\{^{1}H\}$ NMR (202MHz, THF-d_8): δ 4.88 Elem. Anal. Calcd (found) for $C_{40}H_{74}N_2O_5P_4$: C, 61.05 (61.36); H, 9.48 (9.75); N, 3.56 (3.43).

$PN^{Me}P$. The methyl substituted amine (Me) ligand: ^{1}H NMR (500 MHz, CD_3CN): δ 2.61 (d, 4H), 2.37 (s, 3H), 1.37 (q, 8H), 1.03 (tt, 12H). $^{31}P\{^{1}H\}$ NMR (202MHz, CD_3CN): δ -31 (s). Anal. Calcd (found) for $C_{11}H_{27}NP_2$: C, 56.15 (55.78); H, 11.56 (11.78); N, 5.95 (5.74).

General Procedure for the Synthesis of Rhodium Metal Complexes:

To a mixture of $[(COD)_2Rh]BF_4$ in THF (not soluble, 1 mmol) was added a solution of PN^RP ligand (2 mmol) dissolved in THF while stirring. After 1 h, an orange colored solution is obtained. The solvent is removed under vacuum yielding an orange residue which is re-dissolved in ≥ 1 mL of THF then added dropwise to -30 ^{o}C diethyl ether while stirring vigorously. The rhodium complex precipitates as a yellow solid. The mixture is filtered and dried under vacuum yielding analytically pure compound. Metal complexes were prepared in >60% yield.

$[(PN^{AspOMe}P)_2Rh]BF_4$. The AspOMe complex: ^{1}H NMR (500 MHz, THF-d_8): δ 3.87 (t, 2H), 3.71 (s, 6H), 3.63 (s, 6H), 3.07 (dd, 8H), 2.78 (ddd, 4H), 1.84 (m, 16H), 1.19 (m, 24H). $^{31}P\{^{1}H\}$ NMR (202MHz, THF-d_8): δ 2.65 (J_{RhP} = 125.4 Hz).Anal. Calcd (found) for $C_{32}H_{66}BF_4$ $N_2O_8P_4Rh$: C, 41.75 (43.48); H, 7.22 (7.51); N, 3.04 (2.86).

$[(PN^{GlyOMe}P)_2Rh]BF_4$. The GlyOMe complex: ^{1}H NMR (500 MHz, THF-d_8): δ 3.64 (s, 6H), 3.49 (s, 4H), 3.1 (s, 8H), 1.87 (m, 16H), 1.2 (m, 24H). $^{31}P\{^{1}H\}$ NMR (202MHz, THF-d_8): δ 7.04 (J_{RhP} = 125.2 Hz). Anal. Calcd (found) for $C_{26}H_{58}BF_4$ $N_2O_4P_4Rh$: C, 40.22 (40.26); H, 7.53 (7.45); N, 3.61 (3.55).

[(PN^{LeuOMe}P)$_2$Rh]BF$_4$. The LeuOMe complex: ^{1}H NMR (500 MHz, THF-d_8): δ 3.67 (s, 3H), 3.38 (m, 2H), 3.06 (dd, 8H), 1.84 (m, 16H), 1.65 (m, 4H), 1.52 (m, 2H), 1.19 (m, 24H), 0.92 (m, 12H). ^{31}P{^{1}H} NMR (202MHz, THF-d_8): δ 2.33 (J_{RhP} = 125.6 Hz). Anal. Calcd (found) for $C_{34}H_{74}BF_4N_2O_4P_4Rh$: C, 45.96 (46.81); H, 7.84 (7.98); N, 2.94 (2.76).

[(PN^{PheOMe}P)$_2$Rh]BF$_4$. The PheOMe complex: ^{1}H NMR (500 MHz, CD_3CN): δ 7.22 (m, 5H), 4.32 (m, 1H), 3.55 (s, 3H), 3.05 (dd, 4H), 2.69 (dd, 2H), 1.34 (m, 8H), 1.01 (m, 12H). ^{31}P{^{1}H} NMR (202MHz, THF-d_8): δ 2.82 (J_{RhP} = 125.8 Hz). Anal. Calcd (found) for $C_{40}H_{70}BF_4N_2O_4P_4Rh$: C, 50.22 (50.47); H, 7.37 (7.28); N, 2.93 (2.81).

[(PN^{Me}P)$_2$Rh]BF$_4$. –The Me complex: ^{1}H NMR (500 MHz, THF-d_8): δ 2.66 (s, 3H), 2.36 (dd, 4H), 1.78 (m, 8H), 1.13 (m, 12H). ^{31}P{^{1}H} NMR (202MHz, THF-d_8): δ 3.63 (J_{RhP} = 125.2 Hz). Anal. Calcd (found) for $C_{22}H_{54}BF_4N_2P_4Rh$: C, 40.02 (40.07); H, 8.24 (8.34); N, 4.24 (4.15). Crystals of the dihydride complex were prepared by purging a solution in THF with H2. Crystals were clear and prism

General procedure for catalysis. In a dry, nitrogen glovebox, 300 μL d$_8$-THF was used to prepare a solution of catalyst (1.0 mM) and Verkade's base (410 mM – 550 mM, 2,8,9-Triisobutyl-2,5,8,9-tetraaza-1-phosphabicyclo [3.3.3] undecane) at a final volume of 330 μL. A PEEK tube was then charged with this solution and the PEEK cell was fully assembled and isolated before exiting the anaerobic glovebox. Upon attachment to the ISCO high-pressure line, the PEEK cell was evacuated to less than 0.1 torr before refilling with a 1:1 mixture of H_2/CO_2 at a constant pressure of 34 atm. Between kinetic measurements the PEEK cell was placed on a vortex mixer to increase the mixing of gas into the solvent. ^{1}H-NMR & ^{31}P{^{1}H}-NMR spectra were recorded every 3-5 minutes between 2-30 minutes. ^{31}P{^{1}H} NMR chemical shifts in THF-d_8 were referenced to protonated Verkade's base at −11.9 ppm in the absence of CO_2,or −12.9 ppm in the presence of CO_2. To quantify formate production, an external capillary standard ($CoCl_2$, aq, 0.0384 mmol in D_2O) was used inside the PEEK tube and the residual HDO resonance was used as a standard.

Turnover Frequencies (TOFs) were calculated using the initial slope of the kinetic plots. The TOFs reported are the average of a minimum of three kinetic runs.

Electrochemistry. Cyclic voltammetry experiments were conducted at room temperature in a Vacuum Atmospheres glovebox under 1.0 atmosphere of nitrogen or hydrogen. The solvent was THF with 0.1 M tetrabutylammonium tetrafluoroborate ($[TBA]^+[BF4]^-$) as a supporting electrolyte and the potentiostat employed was a CH Instruments CHI620D electrochemical analyzer. A conventional three-electrode electrode configuration was used. A 1.0 mm glassy carbon disk encased in PEEK (Cypress Systems EE040) was used as the working electrode and a glassy carbon rod (Structure Probe, Inc) was used as the counter electrode. Working electrodes were polished with a diamond paste (Buehler) of decreasing size (3.0, 1.0, and 0.25 μm). A pseudo-reference electrode was prepared using a silver wire coated in Cl that was immersed in a solution of THF/$[TBA]^+[BF4]^-$ (0.1 M) and separated from the medium using a VyCor frit. Cyclic voltammetry experiments employed a sweep rate of 0.2 V s^{-1}. All potentials are referenced to the ferrocenium/ferrocene couple at 0 V.

Acknowledgements

This work was supported by the US Department of Energy (DOE), Office of Science, Office of Basic Energy Sciences (BES), Division of Chemical Sciences, Geosciences & Biosciences. A portion of the work (GMC; ligand synthesis) was supported as part of the Center for Molecular Electrocatalysis, an Energy Frontier Research Center funded by the U.S. DOE, Office of Science, BES. Pacific Northwest National Laboratory (PNNL) is operated by Battelle for the U.S. DOE. Pacific Northwest National Laboratory (PNNL) is a multiprogram national laboratory operated for the DOE by Battelle.

References

1. Bachmeier, A.; Armstrong, F., Solar-driven proton and carbon dioxide reduction to fuels—lessons from metalloenzymes. *Curr Opin Chem Biol* **2015**, *25*, 141-151. DOI: 10.1016/j.cbpa.2015.01.001.
2. Creighton, T. E. *Proteins: Structures and Molecular Properties*; 2nd ed.; W.H. Freeman and Company: New York, 1993.
3. Wolfenden, R.; Snider, M. J., The depth of chemical time and the power of enzymes as catalysts. *Acc. Chem. Res.* **2001**, *34*, 938-945.
4. Holm, R. H.; Kennepohl, P.; Solomon, E. I., Structural and functional aspects of metal sites in biology. *Chemical Reviews* **1996**, *96*, 2239-2314.
5. DuBois, D. L., Development of Molecular Electrocatalysts for Energy Storage. *Inorg. Chem.* **2014**, *53*, 3935-3960. DOI: 10.1021/ic4026969.
6. Rakowski DuBois, M.; DuBois, D. L., The Roles of the First and Second Coordination Spheres in the Design of Molecular Catalysts for H_2 Production and Oxidation. *Chemical Society Reviews* **2009**, *38*, 62-72. DOI: 10.1039/b801197b.
7. Fujita, E.; Muckerman, J. T.; Himeda, Y., Interconversion of CO2 and formic acid by bio-inspired Ir complexes with pendent bases. *Biochimica et Biophysica Acta (BBA) - Bioenergetics* **2013**, *1827*, 1031-1038.
8. Appel, A. M.; Bercaw, J. E.; Bocarsly, A. B.; Dobbek, H.; DuBois, D. L.; Dupuis, M.; Ferry, J. G.; Fujita, E.; Hille, R.; Kenis, P. J. A.; Kerfeld, C. A.; Morris, R. H.; Peden, C. H. F.; Portis, A. R.; Ragsdale, S. W.; Rauchfuss, T. B.; Reek, J. N. H.; Seefeldt, L. C.; Thauer, R. K.; Waldrop, G. L., Frontiers, opportunities, and challenges in biochemical and chemical catalysis of CO2 fixation. *Chemical Reviews* **2013**, *113*, 6621-6658.
9. Caserta, G.; Roy, S.; Atta, M.; Artero, V.; Fontecave, M., Artificial hydrogenases: biohybrid and supramolecular systems for catalytic hydrogen porduction or uptake. *Curr Opin Chem Biol* **2015**, *25*, 36-47.
10. Shaw, W. J., The outer-coordination sphere: incorporating amino acids and peptides as ligands for homogeneous catalysts to mimic enzyme function. *Catalysis Reviews: Science and Engineering* **2012**, *54*, 489-550.
11. Ginovska-Pangovska, B.; Dutta, A.; Reback, M. L.; Linehan, J. C.; Shaw, W. J., Beyond the active site: The impact of the outer coordination sphere on electrocatalysts for hydrogen production and oxidation. *Acc. Chem. Res.* **2014**, *47*, 2621-2630. DOI: 10.1021/ar5001742.
12. Dutta, A.; Appel, A. M.; Shaw, W. J., Designing electrochemically reversible H2 oxidation and production catalysts. *Nature Reviews Chemistry* **2018**, *2018*, 244-252.
13. Cardenas, A. J. P.; Ginovska, B.; Kumar, N.; Hou, J.; Raugei, S.; Helm, M. L.; Appel, A. M.; Bullock, R. M.; O'Hagan, M., Controlling Proton Delivery through Catalyst Structural Dynamics. *Angew. Chem. Int. Ed.* **2016**, *55*, 13509-13513. DOI: 10.1002/anie.201607460.
14. Klug, C. M.; Cardenas, A. J. P.; Bullock, R. M.; O'Hagan, M.; Wiedner, E. S., Reversing the tradeoff between rate and overpotential in molecular electrocatalysts for H2 production. *ACS Catal.* **2018**, *8*, 3286-3296.
15. Schwizer, F.; Okamoto, Y.; Heinisch, T.; Gu, Y.; Pellizzoni, M. M.; Lebrun, V.; Reuter, R.; Kohler, V.; Lewis, J. C.; Ward, T. R., Artifical metalloenzymes: reaction scope and optimization strategies. *Chemical Reviews* **2017**, *118*, 142-231.

16. Dutta, A.; Appel, A. M.; Shaw, W. J., Designing electrochemically reversible H2 oxidation andn production catalysts. *Nature Reviews Chemistry* **2018**, *2*, 244-252.
17. Dutta, A.; Ginovska, B.; Raugei, S.; Roberts, J. A. S.; Shaw, W. J., Optimizing Conditions for Utilization of an H2 Oxidation Catalyst with Outer Coordination Sphere Functionalities. *Dalton Transactions* **2016**, *45*, 9786-9793.
18. Dutta, A.; Roberts, J. A. S.; Shaw, W. J., Learning from Nature: Arg-Arg Pairing Enhances H2 Oxidation Catalyst Performance. *Angew. Chem. Int. Ed.* **2014**, *53*, 6487-6491.
19. Dutta, A., Lense, S., Hou, J., Engelhard, M., Roberts, J. A. S., Shaw, W. J., Minimal Proton Channel Enables H2 Oxidation and Produc-tion with a Water Soluble Nickel-Based Catalyst. *Journal of the American Chemical Society* **2013**, *135*, 18490-18496.
20. Lense, S., Dutta, A., Roberts, J. A. S., Shaw, W. J., A Proton Channel Allows a Hydrogen Oxidation Catalyst to Operate at a Moderate Overpotential with Water Acting as a Base. *Chem. Commun.* **2014**, *50*, 792-795.
21. Dutta, A.; DuBois, D. L.; Roberts, J. A. S.; Shaw, W. J., Amino acid modified Ni catalyst exhibits reversible H2 oxidation/production over a broad pH range at elevated temperatures. *PNAS* **2014**, *111*, 16286-16291. DOI: 10.1073/pnas.1416381111.
22. Priyadarshani, N.; Dutta, A.; Ginovska, B.; Buchko, G. W.; O'Hagan, M.; Raugei, S.; Shaw, W. J., Achieving Reversible H2/H+ Interconversion at Room Temperature with Enzyme-Inspired Molecular Complexes: A Mechanistic Study. *ACS Catalysis* **2016**, *6*, 6037-6049. DOI: 10.1021/acscatal.6b01433.
23. Dutta, A.; Lense, S.; Roberts, J. A. S.; Helm, M. L.; Shaw, W. J., The Role of Solvent and the Outer Coordination Sphere on H2 Oxidation Using [Ni(PCy2NPyz2)2]2+. *Eur. J. Inorg. Chem.* **2015**, *2015*, 5218-5225. DOI: 10.1002/ejic.201500732.
24. Fujita, E.; Muckerman, J. T.; Himeda, Y., Interconversion of CO2 and formic acid by bio-inspired Ir complexes with pendent bases. *BBA: Bioenergetics* **2013**, *1827*, 1031-1038. DOI: http://dx.doi.org/10.1016/j.bbabio.2012.11.004.
25. Onishi, N.; Xu, S.; Manaka, Y.; Suna, Y.; Wang, W.-H.; Muckerman, J. T.; Fujita, E.; Himeda, Y., CO 2Hydrogenation Catalyzed by Iridium Complexes with a Proton-Responsive Ligand. *Inorg. Chem.* **2015**, *54*, 5114-5123. DOI: http://doi.org/10.1021/ic502904q.
26. Lilio, A. M.; Reineke, M. H.; Moore, C. E.; Rheingold, A. L.; Takase, M. K.; Kubiak, C. P., Incorporation of Pendant Bases into Rh(diphosphine)2 Complexes: Synthesis, Thermodynamic Studies, And Catalytic CO2 Hydrogenation Activity of [Rh(P2N2)2](+) Complexes. *Journal of the American Chemical Society* **2015**, *137*, 8251-8260. DOI: http://doi.org/10.1021/jacs.5b04291.
27. Schmeier, T. J.; Dobereiner, G. E.; Crabtree, R. H.; Hazari, N., Secondary Coordination Sphere Interactions Facilitate the Insertion Step in an Iridium(III) CO2 Reduction Catalyst. *Journal of the American Chemical Society* **2011**, *133*, 9274-9277. DOI: http://doi.org/10.1021/ja2035514.
28. Bays, J. T.; Priyadarshani, N.; Jeletic, M. S.; Hulley, E. B.; Miller, D. L.; Linehan, J. C.; Shaw, W. J., The influence of the second and outer coordination spheres on Rh(diphosphine)$_2$ CO_2 hydrogenation catalysts. *ACS Catalysis* **2014**, *4*, 3663-3670. DOI: 10.1021/cs5009199.
29. Qi, X.-J.; Fu, Y.; Liu, L.; Guo, Q.-X., Ab initio calculations fo thermodynamic hydricities of transition-metal hydrides in acetonitrile. *Organometallics* **2007**, *26*, 4197-4203.

30. Qi, X.-J.; Liu, L.; Fu, Y.; Guo, Q.-X., Ab Initio Calculations of pKa Values of Transition-Metal Hydrides in Acetonitrile. *Organometallics* **2006**, *25*, 5879-5886. DOI: 10.1021/om0608859.
31. DuBois, D. L.; Blake, D. M.; Miedaner, A.; Curtis, C. J.; Rawkowski DuBois, M.; Franz, J. A.; Linehan, J. C., Hydride Transfer from Rhodium Complexes to Triethylborane. Organometallics. *Organometallics* **2006**, *25*, 4414-4419. DOI: http://doi.org/10.1021/om060584z.
32. Curtis, C. J.; Miedaner, A.; Ciancanelli, R.; Ellis, W. W.; Noll, B. C.; Rakowski DuBois, M.; DuBois, D. L., [Ni(Et2PCH2NMeCH2PEt2)2]2+ as a Functional Model for Hydrogenases. *Inorg. Chem.* **2003**, *42*, 216-227. DOI: 10.1021/ic020610v.
33. El Dine, T. M.; Rouden, J.; Blanchet, J., Borinic Acid Catalysed Peptide Synthesis. *Chem. Commun.* **2015**, *51*, 16084−16087.
34. Lamprecht, D.; Lamprecht, G. J., Electrochemical oxidation of Rh(I) to Rh(III) in rhodium(I) β-diketonato carbonyl phosphine complexes. *Inorganica Chimica Acta* **2000**, *309*, 72-76.
35. Boralugodage, N. P.; Arachchige, R. J.; Dutta, A.; Buchko, G. W.; Shaw, W. J., Evaluating the role of acidic, basic, and polar amino acids and dipeptides on a molecular electrocatalyst for H2 oxidation. *Catal. Sci. Technol.* **2017**, *7*, 1108-1121. DOI: 10.1039/C6CY02579J.
36. Wang, W.-H.; Hull, J. F.; Muckerman, J. T.; Fujita, E.; Himeda, Y., Second-coordination-sphere and electronic effects enhance iridium(iii)-catalyzed homogeneous hydrogenation of carbon dioxide in water near ambient temperature and pressure. *Energy and Environmental Sciences* **2012**, *5*, 7923-7926. DOI: 10.1039/C2EE21888G.
37. Hosseinzadeh, P.; Marshall, N. M.; Chacon, K. N.; Yu, Y.; Nilges, M. J.; New, S. Y.; Tashkov, S. A.; Blackburn, N. J.; Lu, Y., Design of a Single Protein that Spans the Entire 2-V Range of Physiological Redox Potentials. *PNAS* **2016**, *113*, 262-267. DOI: 10.1073/pnas.1515897112.
38. Yu, F.; Cangelosi, V. M.; Zastrow, M. L.; Tegoni, M.; Plegaria, J. S.; Tebo, A. G.; Mocny, C. S.; Ruckthong, L.; Qayyum, H.; Pecoraro, V. L., Protein Design: Toward Functional Metalloenzymes. *Chemical Reviews* **2014**, *114*, 3495-3578. DOI: 10.1021/cr400458x.
39. Benson, E. E.; Kubiak, C. P.; Sathrum, A. J.; Smieja, J. M., *Chemical Society Reviews* **2009**, *38*, 89.
40. Chabolla, S. A.; Machan, C. W.; Yin, J.; Dellamary, E. A.; Sahu, S.; Gianneschi, N. C.; Gilson, M. K.; Tezcan, F. A.; Kubiak, C. P., Bio-inspired CO2 reduction by a rhenium tricarbonyl bipyridine-based catalyst appended to amino acids and peptidic platforms: incorporating proton relays and hydrogen-bonding functional groups. *Faraday Discuss.* **2017**, *198*, 279-300. DOI: 10.1039/C7FD00003K.
41. Schmeier, T. J.; Dobereiner, G. E.; Crabtree, R. H.; Hazari, N., Secondary Coordination Sphere Interactions Facilitate the Insertion Step in an Iridium(III) CO2 Reduction Catalyst. *Journal of the American Chemical Society* **2011**, *133*, 9274-9277. DOI: 10.1021/ja2035514.
42. Yonker, C. R.; Linehan, J. C., The use of supercritical fluids as solvents for NMR spectroscopy. *Progress in Nuclear Magnetic Resonance Spectroscopy* **2005**, *47*, 95-109
43. ; Bruker AXS Inc.: Madison, WI, 2009.
44. ; Bruker AXS Inc.: Madison, WI, 2004; Vol. Vol. 723a.

45. ; Bruker AXS Inc.: Madison, WI, 2001.
46. Sheldrick, G. M., A short history of SHELX. *Acta Cryst.* **2008**, *A64*, 112-122.
47. Sheldrick, G. M.: University of Gottingen, Germany, 2018.
48. Dolomanov, O. V.; Bourhis, L. J.; Gildea, R. J.; Howard, J. A. K.; Puschmann, H., OLEX2: a complete structure solution, refinement and analysis program (pages 339–341). *J. Appl. Cryst.* **2009**, *42*, 339-341.